Rate equations model for semiconductor lasers with multilongitudinal mode competition and gain dynamics

Rate Equations Model for Semiconductor Lasers With Multilongitudinal Mode Competition and Gain Dynamics

Mirvais Yousefi, Alberto Barsella, Daan Lenstra, *Member, IEEE*, Geert Morthier, *Senior Member, IEEE*, Roel Baets, *Member, IEEE*, Stefan McMurtry, and Jean-Pierre Vilcot

***Abstract*—A novel multilongitudinal-mode rate-equations description of the semiconductor laser is presented. The model includes gain interactions among the longitudinal modes due to e.g., spatial hole burning. The parameters have been obtained from a real device, in order to be able to compare with the simulations. The results are in good qualitative agreement with the measurements.**

***Index Terms*—Dynamics, lasers, multilongitudinal mode, semiconductor lasers.**

I. Introduction

THE semiconductor laser has become a key component in modern technology. Among other applications, it is widely used in consumer electronic devices, telecommunication industry, medicine, spectroscopy, and industrial cutting. The complexity of the device varies depending on the area of application, but the general feature is the semiconductor material and a microscopic laser cavity. A full description and modeling of the semiconductor laser would involve complex quantum mechanical level treatment of the semiconductor heterostructure, but generally this leads to computationally heavy calculations that, even when accurate, do not give deep insight into the parameter dependence of such device. Instead, dynamical system models have been proposed [1]–[5] for which the tool of bifurcation theory can be used to investigate the dynamics and its dependence on the parameters. The semiconductor laser is then described by a set of ordinary differential equations, the laser rate equations [6], which capture the most important aspects of the physics of the device, from a single longitudinal mode point of view. In line with this approach, we have developed a multilongitudinal-mode model that describes the semiconductor laser in terms of coupled ordinary differential equations and takes into account competition and gain-dynamics effects among the longitudinal modes.

This model has been developed to address the issue of analyzing the behavior of a semiconductor laser with two laterally coupled Fabry–Perot stripes, where we were confronted with complicated multimode dynamics within and across the stripes [7]. A thorough literature search revealed no fully adequate multimode model applicable to our system.

Manuscript received November 7, 2002; revised April 15, 2003. This work was supported by the European Union through the FALCON European TMR # ERBFMRX-CT98–0223 network.

M. Yousefi is with Vrije Universiteit, FEW, N&S, 1081HV Amsterdam, The Netherlands.

D. Lenstra is with Vrije Universiteit, FEW, N&S, 1081HV Amsterdam, The Netherlands, and also with the COBRA Research Institute, Eindhoven University of Technology, Eindhoven, Netherlands.

A. Barsella, G. Morthier, and R. Baets are with the Department of Information Technology (INTEC), Gent University, B-9000 Gent, Belgium.

S. McMurtry and J.-P. Vilcot are with the Institut d'Electronique et de Microelectronique du Nord, UMR CNRS 8520, Université des Sciences et Technologies de Lille, F-59652 Villeneuve d'Ascq cedex, France (e-mail: vilcot@iemn.univ-lille1.fr).

Digital Object Identifier 10.1109/JQE.2003.816100

II. Description of the Model

It is our goal to present a model that includes the relevant physics of the device while using a minimum number of parameters. Also, the model has to be simple enough to be solvable on a personal computer. This approach is complementary to the full Maxwell–Bloch equations, because one can apply bifurcation theory tools to get an insight into the dynamics of the device and therefore be able to choose the right parameter regions for a further analysis on the basis of a microscopic approach e.g., the complete Maxwell–Bloch model.

We assume that the electrical field inside the device is predominantly single transverse mode. This condition can be met in reality either by the specific laser design or by choosing the correct operation regime for the device, usually by merely adjusting the pump current. The electrical field inside the device can then be written as a longitudinal field

$$\mathcal{E} = \mathcal{E}(z,t) = \sum_{j=1}^{j=M} E_j(t)\psi_j(z)e^{i\omega_j t} + c.c. \tag{1}$$

Here, we have decomposed the total field $\mathcal{E}(z,t)$ into its longitudinal mode components, M of which are assumed to be active, while all remaining longitudinal modes have negligible power. The frequencies of the M modes $\{\omega_j\}_{j=1}^{M}$ can in principle be chosen freely, as long as that choice leads to field amplitudes $E_j(t)$ that are weakly time-dependent. In this respect, "weak" means that the dynamics of the resulting amplitude should fall within a range much smaller than the longitudinal mode spacing. The frequencies $\{\omega_j\}_{j=1}^{M}$ will be fixed later on [see (4)]. $\psi_j(z)$ is the longitudinal spatial profile of the jth mode. We assume the $\{\psi_j(z)\}_{j=1}^{M}$ to be orthogonal and normalized, i.e., $\int_0^L dz\psi_j^*(z)\psi_k(z) = \delta_{jk}$, where L is the device length. The local number of electron-hole pairs (inversion) is denoted by $N(z,t)$. N is normalized such that $N = 1/L\int_0^L dzN(z)$ equals the total number of electron-hole

pairs in the device. The spatial distribution of the carriers will depend on the field dynamics and device design. We split the inversion among the longitudinal modes, so that each slowly varying envelope has its corresponding inversion moment. These inversion moments will "feed from a common pot" and this leads to coupled dynamics that will be treated further down. The inversion moments are defined as

$$n_j(t) \equiv \int_0^L dz|\psi_j(z)|^2(N(z,t)-\overline{N}) \tag{2}$$

where $\overline{N} \equiv 1/L\int_0^L dz N_{\rm thr}(z)$, i.e., the total number of carriers at the highest pump current $J_{\rm thr}$ for which no laser action occurs. The threshold of the lowest loss longitudinal mode is taken as the reference point, since here the modal frequencies $\{\omega_n^0\}_{n=1}^M$ are uniquely defined. According to (2) the longitudinal modes give rise to an *inversion grating* created in the device expressed by the inversion moments $\{n_n(t)\}_{n=1}^M$.

The gain profile depends on the frequency, which drifts with the operation parameters, and on the inversion, which varies with the dynamical state of the device. Ideally, a full dynamical description of the gain would require using a self-consistent analysis, in which the device gain is recalculated at each integration step using the current states of field and carriers as the input. However, since we focus on relatively slow dynamics ($\sim$ 20 GHz, i.e., $\sim$ 50 ps) compared to the intraband carrier relaxation dynamics of the semiconductor material ($\geq$ 1 THz i.e., $\leq$ 1 ps), it is reasonable to assume that the polarization, i.e., induced dipole-moment density, is in quasiequilibrium, so that it can be eliminated adiabatically from the equations. Spatial diffusion of carriers is present and, ideally again, should be described by a diffusion equation. However, this will complicate the model too much and we choose instead, to account for the diffusion through an effective description as introduced below. We linearize the gain with respect to the inversion and neglect frequency dependence of the parameters for the dynamical region of interest($\sim$ 20 GHz) . The gain of the jth mode can then be expressed as [17]

$$G_j = \frac{1}{2}g_j + \frac{1}{2}\xi_j(1+i\alpha_j)n_j(t) \tag{3}$$

where ξ_j is the differential gain coefficient of the jth mode, α_j its linewidth-enhancement factor that accounts for the self-phase modulation effects of semiconductor laser, and g_j is the modal gain at the threshold of the lowest loss-mode.

We fix now the modal frequencies $\{\omega_j\}_{j=1}^M$ introduced above (1). They will vary as the operation parameters (temperature, pump-current) are changed. We assume that the device is in thermal equilibrium and attribute all frequency drifts within the interval of interest to the pump current through the empirical relationship

$$\omega_j = \omega_j^0 - \kappa_j \Delta J \tag{4}$$

where κ_j is a positive dimensionless parameter accounting for the total pump-dependent frequency drift of the jth mode which includes both band-gap-shrinkage effects, temperature-induced drift and changes due to variations in the index of refraction. This parameter can be measured by using a reference frequency and recording the pump-induced modal-frequency drift. In (4), $\Delta J \equiv J - J_{\rm thr}$, where J is the pump rate and $J_{\rm thr}$ is the threshold pump rate of the lowest loss mode. Finally, ω_j^0 is the reference optical frequency of mode j measured at the threshold of the lowest loss mode.

The rate equations for the slowly varying envelope of each longitudinal mode and its inversion moments can now be written as

$$\dot{E}_k(t) = \frac{1}{2}(1+i\alpha_k)\xi_k n_k(t)E_k(t) + \frac{1}{2}(g_k-\Gamma_k)E_k(t) \tag{5}$$

$$\dot{n_k}(t) = \Delta J - \frac{n_k(t)}{T} - \sum_{l=1}^{M} f_{k,l}|E_l(t)|^2(g_l+\xi_l n_l(t)). \tag{6}$$

Here, the pump rate above threshold ΔJ is assumed to be the same for all modes (uniform pumping), where T is the spontaneous-recombination carrier decay lifetime and ${\Gamma_k}^{-1}$ is the cavity lifetime of the photons (losses) in mode k. As a consequence of our definition of the reference point $\overline{N}$, the threshold gain of the lowest loss mode exactly compensates for the optical losses in that mode, i.e., $g_1 = \Gamma_1$, while for all other modes, the losses will be greater than the threshold gain, $g_k < \Gamma_k, k = 2,3\ldots M$. The first term in (5) accounts for the real and imaginary part of the stimulated emission gain, while the second term accounts for the net optical loss of mode k. By definition, the latter term vanishes for $k=1$. $f_{k,l}$'s are the weights describing the modal inversion dynamics and are usually dependent on the specific laser design. The main difference between our model and that presented in [14] is that the latter model has fixed gain dynamics where the inversion moment of mode k only feels itself and the total output power. In (6), the inversion moments are coupled to *all* other inversion moments. This makes gain competition and mode suppression possible and highly nontrivial. However, we strongly believe that our model as expressed by (6) is more realistic as to the mode competition dynamics. According to (5), the gain of mode k is provided by the kth inversion moment, while (6) describes the fact that the kth inversion moment suffers from depletion not only due to its own corresponding mode ($f_{k,k}$) but, since all other modes are eating from the total inversion as well, also from the feeding of the other modes ($f_{k,l}$).

The gain suppression co-efficients $f_{k,l}$'s are defined as

$$f_{k,l} = \frac{1}{L}\int_0^L dz|\psi_k(z)|^2|\psi_l(z)|^2 \tag{7}$$

and can be evaluated when the spatial profiles are known. In the special case of sine functions, i.e., $\psi_l(z) \equiv \sqrt{(2/L)}\sin(n_l\pi z/L)$, $n_l \in \mathbf{N}$, it is straightforward to show that $f_{k,l} = 1/2 + \delta_{kl}/4$, where δ_{kl} is the Kronecker delta. Since the spatial profiles are generally not sine waves, we will use the above result as an indication on the $f_{k,l}$ values and restrict these to $0 \leq f_{k,l} \leq 1$. It is interesting to note that by deviating from the sine values of the $f_{k,l}$'s, one also effectively accounts for carrier diffusion. The effect of diffusion is to "wash out" the inversion grating and thus effectively change the couplings between the slowly varying envelopes of the field and their inversion moments.

It should be noted that (5) can be derived from the paraxial equations for the semiconductor laser [17] and that in deriving (6) we have performed certain approximations. For example, we have assumed that one set of $f_{k,l}$'s is sufficient to describe the gain-dynamics, while a full derivation results in two sets of $f_{k,l}$'s. One set that multiplies the g_l in the sum and the other set of $f_{k,l}$'s appear in a product with the $\xi_l n_l(t)$ term within the sum in (6). To some extent, we can correct eventual errors introduced by this approximation in the values of g_l. In this sense, we will calibrate the ξ_l's to measurements and use the g_l's as "free parameters".

In (5) and (6), the specific device properties are reflected in the parameter set: $\{\{\alpha_k\},\{\xi_k\},\{g_k\},\{\Gamma_k\},\{f_{jk}\},T,\Delta J\}$ where $j,k=1,\ldots,M$. It is beyond the scope of this paper to analyze the dependence of the dynamics on the whole parameter set. Instead, in the next chapter we will present an overview of how the most important parameters affect the dynamics. First, we set the gain dynamics by adjusting $\{g_n,\xi_n,\alpha_n\}_{n=1}^{M}$ and choose the modal losses Γ_n equal for all modes, normally a good approximation. Then the type of laser is decided on by adjusting the $f_{k,l}$ values so as to achieve correct mode-resolved pump-intensity (PI) characteristics. To make this procedure transparent, we start the analysis by paying special attention to the two-active-mode scenario, so as to identify the different steps in the calibration process in a very simple environment.

III. Theoretical Analysis

For a single-mode semiconductor laser with $M=1$ and $f_{1,1}=1$, (5) and (6) reduce to the standard laser rate equations [6] as follows:

$$\dot{E}(t)=\frac{1}{2}(1+i\alpha)\xi n(t)E(t) \tag{8}$$

$$\dot{n}(t)=\Delta J-\frac{n(t)}{T}-|E(t)|^2(g+\xi n(t)) \tag{9}$$

where we have dropped the index for simplicity. Let us give a short summary of the single-mode case before we address the situation with two modes. The single-longitudinal-mode semiconductor laser model is well understood [1]–[4]. Steady-state analysis shows that there are two possible states of operation: the on state and the off state. Below threshold (i.e., $\Delta J<0$), the off state is the only state and it is stable. Above threshold, the off state has one positive (unstable) and one negative (stable) eigenvalue, meaning that the slightest fluctuation in power and/or inversion will drive the system to the on state, which has two negative eigenvalues. The laser-threshold transition is an example of the transcritical bifurcation [12].

A. The Case of Two Modes

It is instructive to pay special attention to the two-mode case in order to clarify the relevance of the different parameters. We will first determine the fixed points for this case and their stability. We consider the two-mode case to be a first approximation for multimode operation. In this spirit, the condition for the onset of two-mode operation that will be derived, should be seen as a crude indication of the multimode situation.

For the fixed-point analysis, it is convenient to rewrite (5) and (6) in terms of power $P_j(t)$ and phase $\phi_j(t)$, $E_j(t)=\sqrt{P_j(t)}e^{i\phi_j(t)}$. $P_j(t)$ corresponds to the total number of photons in mode j. In terms of these variables, (5) and (6) read

$$\dot{P}_k(t)=(g_k-\Gamma_k)P_k(t)+\xi_k n_k(t)P_k(t) \tag{10}$$

$$\dot{\phi}_k(t)=\frac{1}{2}\alpha_k\xi_k n_k(t) \tag{11}$$

$$\dot{n}_k(t)=\Delta J-\frac{n_k(t)}{T}-\sum_{l=1}^{2}f_{k,l}P_l(t)(g_l+\xi_l n_l(t)) \tag{12}$$

where $k=1,2$. From (11), it clearly follows that for each mode, the phase is not an independent variable but a follower of the inversion moment. The nontrivial dynamics takes place in the four-dimensional phase space spanned by the modal powers and the inversion moments. We define the states of CW operation as the fixed points of our system, since during CW operation, the power and the inversion do not change ($\dot{P}_j(t)=\dot{n}_j(t)=0$), while the frequency is fixed, i.e., $\dot{\phi}_j(t)=\overline{\omega}_{s,j}$, where $\overline{\omega}_{s,j}$ is the frequency shift of the jth mode with respect to ω_j. The fixed-points ansatz reads

$$E_j(t)=\sqrt{\overline{P}_j}e^{i\overline{\omega}_{s,j}t} \tag{13}$$

$$n_j(t)=\overline{n}_j \tag{14}$$

where $\overline{P}_j,\overline{\omega}_{s,j},\overline{n}_j\in\mathbf{R}$, $\overline{P}_j>0$, and $j=1,2$. This corresponds to continuous-wave (CW) operation of the jth mode with output power corresponding to $\overline{P}_j$ photons in the cavity with frequency $\overline{\omega}_{s,j}$. Inserting (13) and (14) into (10) and (12) will result in four distinct situations:

i) both modes off;
ii) mode 1 on and mode 2 off;
iii) mode 2 on and mode 1 off;
iv) both modes on.

To perform a stability analysis, for each fixed-point solution we calculate the Jacobian matrix. The eigenvalues of this Jacobian reveal the stability properties of the system at that fixed point. Since the method is standard, we briefly summarize the outcome of the analysis.

Intuitively, it is clear that the off-state [case (i)] will be stable below threshold and destabilize once the pump current is above threshold. The eigenvalues confirm this and, in fact, they show that a second eigen-direction will become unstable once the pump current is large enough to compensate the losses in the second mode and pull it above its threshold, i.e., $\Delta J\geq(\Gamma_2-g_2)/(\xi_2 T)$. Hence, solution 1) is stable below threshold and for $\Delta J>0$ the dynamics of the system will drive the laser into one of the scenarios 3)-4).

In case (ii), the lowest loss mode is on, $\overline{P}_1=\Delta J/(g_1 f_{1,1})>0$ above threshold, while the other is off, $\overline{P}_2=0$. The inversion moment of mode 1 is clamped to zero and the off-mode inversion is given by

$$\overline{n}_2=\frac{\Delta JT(f_{1,1}-f_{2,1})}{f_{1,1}}. \tag{15}$$

Since the ratio of the $f_{k,l}$'s will turn out to be decisive for the stability in general, we define

$$\delta f_{j,k} \equiv \frac{f_{k,k} - f_{j,k}}{f_{k,k}} \leq 1. \tag{16}$$

Note that the quantity of interest for mode 1 is $\delta f_{2,1}$ while that of mode 2 is $\delta f_{1,2}$. The stability analysis shows that two of the four eigenvalues for case (ii) are a conjugate pair and can become complex-valued, but they correspond to stable behavior since their real parts are always negative. One eigenvalue is always negative while the last one is negative as long as

$$\Delta J \xi_2 T \delta f_{2,1} - \Gamma_2 + g_2 \leq 0. \tag{17}$$

If this inequality is broken, then one of the eigenvalues becomes positive, leading to an instability. Therefore, the fixed-point scenario 2) will be stable so long as the pump current and $\delta f_{2,1}$ are such that (17) holds.

In case (iii) mode 1 is off, $P_1 = 0$, and the values of the other variables are

$$\overline{P}_2 = \frac{\Delta J - \frac{\Gamma_2 - g_2}{\xi_2 T}}{\Gamma_2 f_{2,2}} \tag{18}$$

$$\overline{n}_1 = T \Delta J \delta f_{1,2} + (1 - \delta f_{1,2}) \frac{\Gamma_2 - g_2}{\xi_2} \tag{19}$$

$$\overline{n}_2 = \frac{\Gamma_2 - g_2}{\xi_2}. \tag{20}$$

Since $P_2 \geq 0$, an expression for the threshold of the second mode can be derived from (18)

$$\Delta J \geq \frac{\Gamma_2 - g_2}{\xi_2 T} \equiv J_{\mathrm{thr}2}. \tag{21}$$

If the pump current is larger than $J_{\mathrm{thr}2}$, then the losses of the second mode can be overcome and operation in this state becomes possible. The stability analysis reveals that in accordance with case (ii), two of the four eigenvalues are conjugate pairs with a negative real part which do not change sign as the pump current or $\delta f_{1,2}$ is varied above the threshold of mode 2 ($J_{\mathrm{thr}2}$). The third eigenvalue is always negative, but the fourth can change sign.

For the stable operation in scenario 3), i.e., negative eigenvalues and $P_2 \geq 0$, the pump current must obey the following two inequalities at the same time:

$$\frac{\Gamma_2 - g_2}{\xi_2 T} \leq \Delta J \tag{22}$$

$$\Delta J \delta f_{1,2} \leq \frac{g_2 - \Gamma_2}{T \xi_2} (1 - \delta f_{1,2}) \tag{23}$$

where the upper limit has been derived from the stability analysis. Note that this limit differs from (17) and that (23) states that case (iii) can only be stable for negative $\delta f_{1,2}$.

In multimode operation [case (iv)], both inversion moments will be clamped to the threshold value of the specific mode $n_1 = 0$, $n_2 = (\Gamma_2 - g_2)/\xi_2$. Due to its lower losses, mode 1 will start lasing first and grow with the pump current, while mode 2 will lase once its threshold losses have been overcome. This is expressed as

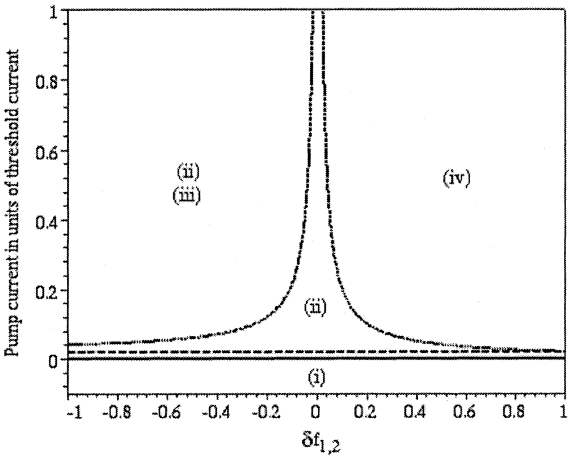

Fig. 1. Regions of different dynamics in the $(\delta f_{1,2}, \Delta J)$-plane as derived from the analysis in Section III-A. The symbols (i)-(iv) identify different operation (see text).

$$\overline{P}_1 = \frac{\Delta J}{\Gamma_1 f_{1,1}} \tag{24}$$

$$\overline{P}_2 = \frac{1}{\Gamma_2 f_{2,2}} \left(\Delta J \delta f_{2,1} - \frac{\Gamma_2 - g_2}{\xi_2 T} \right) \tag{25}$$

which implies that the lower stability limit of case (iv) coincides with (17).

Fig. 1 summarizes the stability boundaries of all four fixed points-cases as identified from (17), (21), (22), and (23) and the eigenvalue analysis. In this figure, we have restricted the analysis to the special symmetric case of $f_{2,1} = f_{1,2}$ and $f_{1,1} = f_{2,2}$ in order to be able to display the results in the $(\delta f_{1,2}, \Delta J)$-plane rather than the $(\delta f_{1,2}, \delta f_{2,1}, \Delta J)$-space. All other parameter values are listed in Table I.

Below threshold ($\Delta J \leq 0$), case (i) is the only stable solution, while for $0 < \Delta J \leq J_{\mathrm{thr}2}$ only mode 1 can be excited and this correspond to operation in case (ii). Once $\Delta J > J_{\mathrm{thr}2}$, there are enough carriers in the device to potentially maintain operation in both modes, but for our choice of parameters this does not happen immediately, since according to (15) the on-mode actually reduces the off-mode's inversion, and thus increases the effective threshold for mode 2.

Let us now study the stability boundaries from right to left in Fig. 1 for $\Delta J > J_{\mathrm{thr}2}$. At the far right ($\delta f_{1,2} = 1$), each mode is not coupled to the inversion moment of the other mode, while it is strongly coupled to its own inversion moment. This corresponds to two independently lasing modes in the laser. Now, moving further to the left the first boundary one encounters is the border between regions (ii) and (iv). Only multimode operation can be sustained in region (iv). At $\delta f_{1,2} = 0$, each mode is equally strongly coupled to the inversion moments of all other modes including its own. This implies that all modes feed from one "global" inversion moment, meaning that no intra-modal suppression occurs. Most existing multimode models are restricted to this $\delta f_{1,2} = 0$ region. Until the next boundary to the left, only case (ii) is stable.

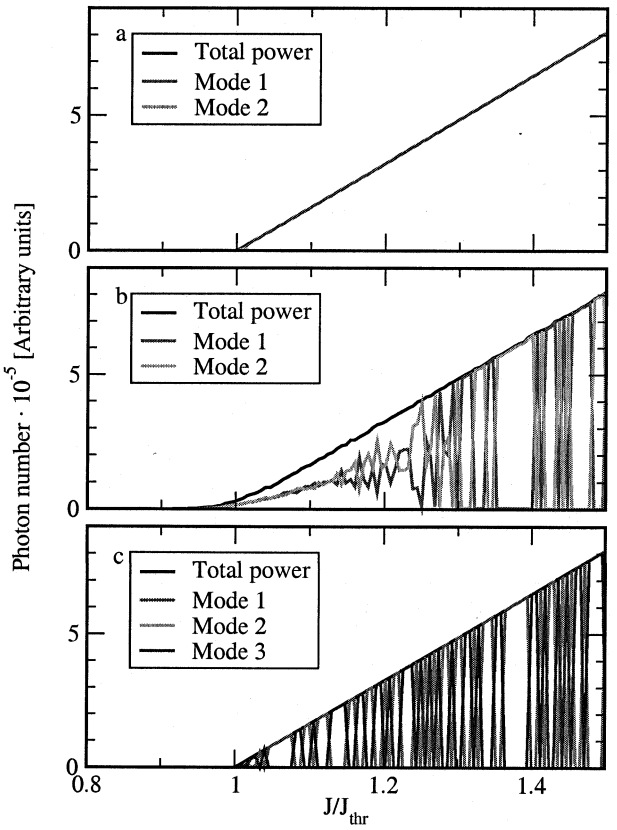

Fig. 2. Simulated pump-intensity curves for two active modes (a) and (b) and three active modes (c). In (b) and (c), spontaneous emission noise has been included. The noise induces spontaneous switching between the stable states and thus illustrates the bistability.

Continuing further to the left we encounter the boundary defined by (23) and case (iii) stabilizes. This is a bistable region where both (ii) and (iii) are stable. Here, the final state of operation will depend on the initial conditions. The single-mode bistable region is restricted to the negative $\delta f_{2,1}$ values which can be understood as follows: when $\delta f_{2,1}$ is negative, the specific mode is using more of the neighboring modes carriers than its own. Therefore, once a mode is excited in this region, it will suppress the other mode by consuming its carriers. In a simulation, the initial conditions will be decisive for the final state, (ii) or (iii). Fig. 1 shows that even in the simple scenario of two active modes, the model shows rich dynamics and complicated mode-competition together with a large parameter range with multistable behavior. The boundaries between the different regions can experimentally be investigated by varying the pump current at fixed $\delta f_{2,1}$. This corresponds to a straight vertical line in Fig. 1.

In the following, we will present simulations for which we have used a fourth-order Runge–Kutta to integrate (5)–(6) and a second-order Runge–Kutta method when noise was included. The integration step size was set to 0.1 ps. At each pump current value, an average is taken over 50 ns after a 50-ns transient has been disregarded. The results will be presented as PI curves such as Fig. 2(a). Noise has been included by means of Langevin force in the standard manner [13]. It is assumed

TABLE I
PARAMETER VALUES USED IN FIG. 1

Parameter	Value	Description
α_1	3.5	Line width enhancement factor
α_2	3.5	Line width enhancement factor
ξ_1	$1 \cdot 10^3\ s^{-1}$	Differential gain coefficient
ξ_2	$1 \cdot 10^3\ s^{-1}$	Differential gain coefficient
Γ_1	$1 \cdot 10^{11}\ s^{-1}$	Photon decay rate
$J_{\rm thr}$	$1.62 \cdot 10^{17}\ s^{-1}$	Threshold pump rate
T_1	1 ns	Carrier life time

that the shot noise and the spontaneous emission noise are uncorrelated, which is reasonable since the spontaneous emission rate into the lasing mode is usually very small ($\beta \sim 10^{-5}$) . Each longitudinal mode feels an independent noise event, which corresponds to a spontaneously emitted photon into the lasing mode. The spontaneous emission rate is set to $R = 5 \cdot 10^{12} s^{-1}$ and the inversion diffusion rate is set to $D_{NN} = J, J < J_{\rm thr}$ and $D_{NN} = J_{\rm thr}, J > J_{\rm thr}$. We also assume that all inversion moments feel the *same* noise event. The noise is generated by a standard Gaussian-noise generator [15] that returns a Gaussian-distributed random number with zero mean and standard deviation of 1.

In Fig. 2(a), the pump-intensity curve is shown for $\delta f_{1,2} = -0.02$ (and $\delta f_{2,1} = -0.02$ due to our choice of symmetric parameters) and $\Gamma_2 - g_2 = 0$. The rest of the parameters are stated in Table I. This choice of parameters means that $J_{\rm thr2} = 0$ and that the two modes will have equal gain meaning that in Fig. 1 the $J_{\rm thr2}$ boundary coincides with the $\Delta J = 0$ line and that the two other boundaries will asymptotically approach the y-axis. Therefore, it is the $f_{k,l}$ settings alone that will decide the intra-modal dynamics. Physically, this corresponds to a multimode Fabry–Perot type laser where two modes are active at threshold and the gain dynamics is such that both modes try to compete by depleting each others inversions, e.g., $f_{k,k} < f_{j,k}$. But since the difference is so small, i.e., $\delta f_{1,2} = -0.02$, several dynamical behaviors can be expected and the laser is on the edge of multimode operation.

As the laser approaches threshold in Fig. 2(a), the multimode region is entered at once. When the pump current is increased further, the laser enters the bistable (ii)-(iii) region where the final state of operation is decided by the initial conditions. Since no noise is included in the simulations for Fig. 2(a), the system remains on the same fixed point and no mode switching is present. In Fig. 2(b), noise has been included in the simulation while the rest of the parameters are the same as Fig. 2(a). Noise effectively extends the multimode region over a larger current range ($\sim 1.2 J_{\rm thr}$). Thereafter, spontaneous switching occurs between the two possible states of operation [cases (ii) and (iii)] as the pump current is increased further. Since spontaneous emission provides excess photons to each mode, the power of the second mode remains positive in a larger region than expressed by (25). The boundaries between region (iv) and (iii) as well as between (ii) and (iii) are not sharp anymore and

smooth transitions take place [see $\Delta J \sim 1.2$ in Fig. 2(b)]. In any case, in regions just above threshold, the presence of noise is known to alter the configuration of fixed points and their stability. Even for a single-mode situation, noise drastically changes the bifurcation structure near threshold: while a transcritical bifurcation occurs at threshold without noise, no bifurcation at all occurs with noise. Thus, similar things are expected to happen in the two-mode case near the bifurcation lines in Fig. 1 when noise is present.

In general, a real laser is much more complex than the simple two-mode analysis presented here. But this section illustrates the richness of the model even for a two-active-modes scenario. As the number of modes increases, the map as presented in Fig. 1 becomes more complex, but that analysis will be beyond the scope of this paper. As an example of that complex dynamics, we present in Fig. 2(c) a PI curve for three active modes, where the $f_{k,l}$'s have been chosen such that a bistability exists between mode 1 and mode 3 while mode 2 is unstable. Noise has been included in the simulations to illustrate the spontaneous switching between the two stable states.

IV. Application to Real Lasers

Our device is a typical ridge structure Fabry–Perot laser. Its epilayers are grown on $n+$ type InP substrate by gas source molecular beam epitaxy. The active medium is composed of six GaInAsP, compressively strained ($+0.7\%$). The top $p+$ type InP confinement layer is 2.5 μm thick. The ridge structure is obtained by etching this confinement layer down to 0.4 μm above the active layer. The ridge width is 4 μm and is delimited by wet etching and using the previously deposited p-type electrode mask. A Dow Chemicals Cyclotene™ resin (BCB 4626–46) is used as planarization layer. Contact pad is then deposited in order to connect p-type electrode. Backside thinning and metallization end the fabrication process. The wafer is then cleaved into 300-μm-long bars which delimit the Fabry–Perot cavities. A more detailed description of the fabrication process can be found in [16].

A. Setup

The device is mounted on a temperature-controlled support, which is cooled by a Peltier junction to ensure a constant operation temperature of 20 °C. A stabilized current source is used to apply the bias current to the device. The diode's output is sent through an objective to shape the beam and couple it into a GRIN-lens single-mode fiber. An optical isolator is placed before the fiber entry point to prevent external cavity feedback effects. The fiber can be connected to a multitude of measurement equipment to examine the device's behavior. In particular, we used relative intensity noise (RIN) measurements to obtain the relaxation oscillations frequency, and the optical spectrum to track the longitudinal mode wavelength and power distribution. By scanning the current source, we have recorded the evolution of those variables as a function of the bias current. All the instruments were connected to a PC for data recording and subsequent analysis.

The PI curves were extracted from the optical spectrum by first identifying the active longitudinal modes, seven in our case.

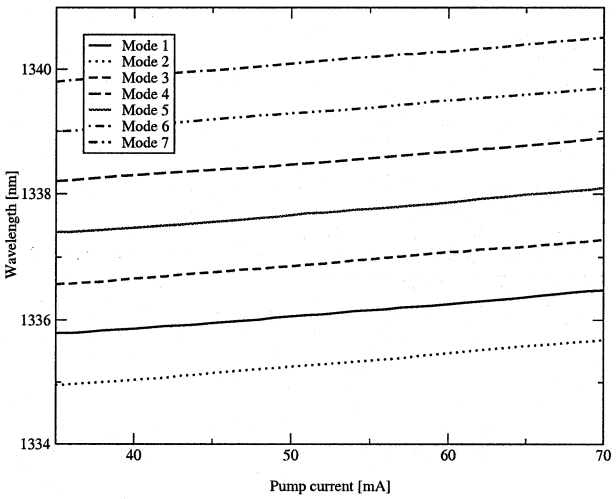

Fig. 3. Measured pump-induced frequency drift of the seven active modes in the laser.

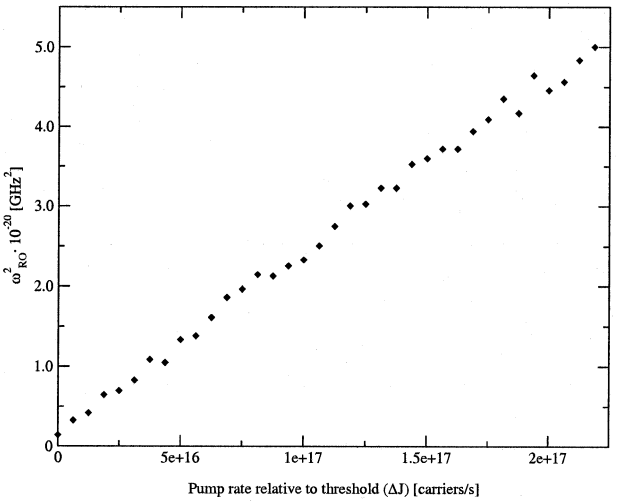

Fig. 4. Measured relaxation oscillation frequency of the main mode squared versus the pump rate relative to threshold. The slope of the curve is ξ (the differential gain coefficient).

The powers were then assumed to be proportional to the amplitude of the spectral line of the specific longitudinal mode, and these lines were tracked through the current-dependent optical spectrum to create mode-resolved PI curves as presented in Fig. 6. The limitation of our accuracy is set by the resolution of the spectrum analyzer and the number of currents points we choose to investigate. Also, the choice of *active* longitudinal modes is very subjective, which can be realized from the slightly uneven PI curve for the total power in the bottom panel of Fig. 6.

B. Extraction of Parameters and Simulations

The measurements described in the previous section are shown in Figs. 3–6. From the full optical spectrum (not shown), we identify seven main longitudinal modes and a total of approximately 25 active longitudinal modes in the device. The dominant modes are clustered around the same frequency region and they drift to lower frequencies as the pump current is increased from 35 mA (threshold) to 70 mA.

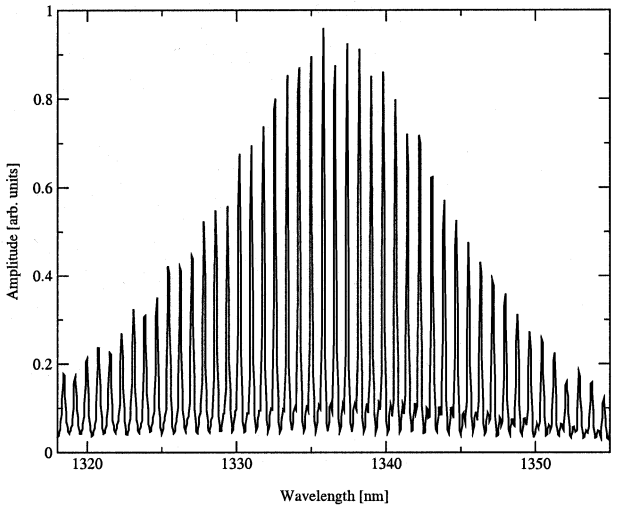

Fig. 5. ASE spectra measured at 30 mA. It is assumed that the modes drift negligibly in the interval up to threshold, and therefore $\{\omega_n\}_{n=1}^{n=7}$ can be extracted from this plot.

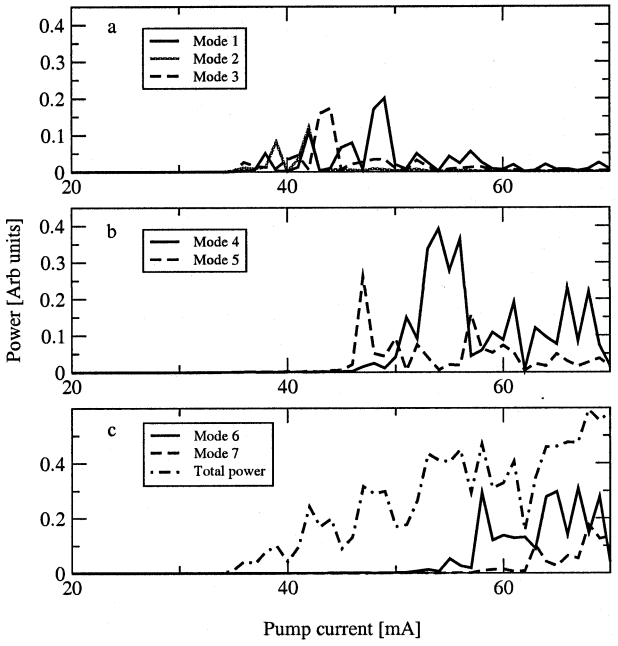

Fig. 6. Experimental mode-resolved PI curves of the laser. The seven modes have been divided between the three panels for the sake of clarity. In the lowest panel, the total power (sum of the seven active modes) is also indicated.

To simplify the analysis, we will "guess" some of the parameters and fix them to realistic values. We set $\alpha_n \equiv \alpha$, $n = 1 \ldots M$, with $\alpha = 3.5$, $\Gamma = 10^{11}$ s^{-1} and $T = 1$ ns. Other parameters $\{\xi_n, g_n, \omega_n^0\}_{n=1}^{M}$ will be extracted from measurements and at the end we will adjust the $f_{k,l}$'s so as to achieve the correct PI characteristics.

As mentioned, from the full optical spectrum above threshold, we identify seven active modes in the range [35,70] mA. Since the optical spectrum has been measured at each 1 mA interval within this range, we can extract the pump-induced frequency shift. In Fig. 3, we show the wavelength dependence of the dominant modes as a function of the bias current. Fitting a linear

TABLE II
PARAMETER VALUES DERIVED FROM THE MEASUREMENTS ($q = 1, 2 \ldots 7$). FOR THEIR DESCRIPTION, SEE TABLE I

Parameter	Value
Γ_q	$\{0.1, 0.1, 0.1, 0.1, 0.1, 0.1, 0.1\} \cdot 10^{12} s^{-1}$
g_q	$\{0.1, 0.099, 0.098, 0.092, 0.09, 0.08, 0.05\} \cdot 10^{12} s^{-1}$
ω_q^0	$\{1335.8, 1335, 1336.6, 1338.2, 1337.4, 1339, 1339.8\} nm$
T_1	$1.0 \cdot 10^{-9}$ S
α_q	$\{3.5, 3.5, 3.5, 3.5, 3.5, 3.5, 3.5\}$
ξ_q	$\{2.351, 2.230, 2.230, 2.270, 2.270, 2.226, 2.108\} \cdot 10^3 s^{-1}$
J_{thr}	$1.4 \cdot 10^{17} s^{-1}$

TABLE III
$f_{k,l}$-VALUES USED TO PRODUCE FIG. 7

	1	2	3	4	5	6	7
1	1.01	1.02	1.02	1.02	1.02	1.02	1.02
2	1.02	1.02	1.02	1.02	1.02	1.03	1.03
3	1.02	1.02	1.02	1.02	1.02	1.03	1.03
4	0.85	0.85	0.85	0.9	0.85	0.885	0.885
5	0.85	0.85	0.85	0.85	0.9	0.885	0.885
6	0.88	0.88	0.686	0.686	0.686	0.7	0.686
7	0.88	0.88	0.686	0.686	0.686	0.686	0.7

curve to the different modes indicates that a linear approximation with the same $\kappa = 5.737 \cdot 10^{-7}$ radians per carrier, the coefficient for all modes correctly reproduces the measurements.

The relaxation oscillation frequency of a single-mode laser (8)–(9) is related to the pump rate as $\omega_{RO} = \sqrt{\xi \Delta J}$[17]. In Fig. 4, ω_{RO}^2 is plotted versus the pump rate above threshold. Again, by a linear fit to this curve, we obtain $\xi = 2351 \pm 16\,\text{s}^{-1}$. We set the differential gain coefficient of the main mode at 2351 s^{-1} and will calibrate the side modes relative to this value by means of the amplified spontaneous emission (ASE) spectrum. The gain of the device is reflected in the ASE spectrum below threshold (Fig. 5). We use this ASE figure to set $\{\omega_n\}_{n=1}^{7}$ and to calibrate the rest of the ξ_n's relative to ξ_1. The resulting values are listed in Table II, where we have used the relative amplitudes of the peaks in Fig. 5 to arrive at the gain spectrum of this table.

Finally, we use the measured full optical spectrum to create a mode-resolved PI curve as described in the previous section. This is shown in Fig. 6. The g_n's are now adjusted "by hand" by identifying the threshold of each mode, as was done for the two-mode case in (21).

The modal dynamics can now be set by adjusting the $f_{k,l}$'s. In our case, we have simply "guessed" the $f_{k,l}$'s since the full analysis would involve a 21-dimensional stability analysis. The $f_{k,l}$ values are listed in Table III and the resulting PI curves are shown in Fig. 7. In these calculations, we have set the $f_{k,l}$'s so as to achieve three active modes with some mode competition at threshold, two simultaneously active modes at the intermediate currents (middle panel), and two simultaneously active modes with asymmetric powers far above threshold. Although the exact

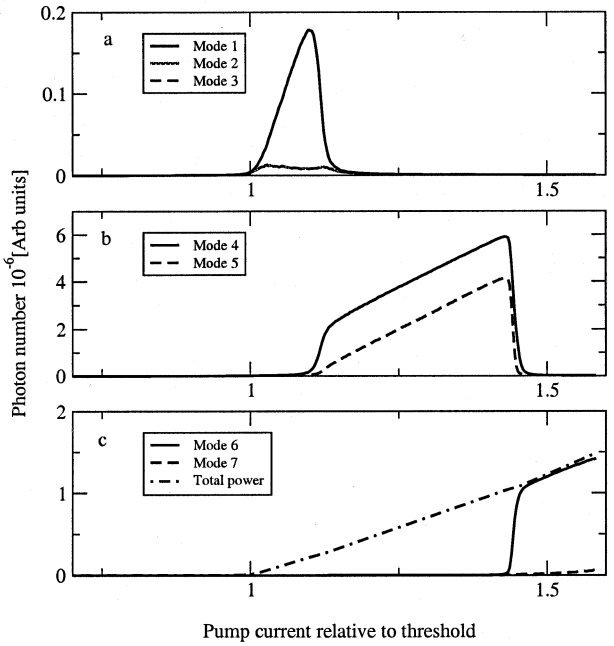

Fig. 7. Theoretical mode-resolved PI curves of the laser.

power levels do not match the experimental values, the gain-induced mode dynamics of the device can be reproduced quantitatively. For an exact reproduction of the experiment, we believe that an full stability analysis of the seven-mode case should be performed and the $f_{k,l}$-parameters set thereafter.

In Fig. 7, spontaneous emission noise was included in the calculations and an average was taken over 50 ns at each current step. The system is in CW operation throughout the scanning range, and the first mode switch is smoother than the second, abrupt mode switch (panel b to c) which can be seen from the total power curve which shows a kink at the second mode switch. The type of switching was chosen by adjusting the $f_{k,l}$ values.

V. Conclusion and Discussions

We have presented a new multilongitudinal mode description for a Fabry–Perot type semiconductor laser in terms of ordinary differential equations, complementary to the more usual description of multimode dynamics of a semiconductor laser in terms of partial differential equations that account for spatial effects. We have introduced the concept of *modal inversion moments* and removed the spatial dependence from the description. To do this, we used the standard approximation of the spatial profiles of the longitudinal modes as standing waves in the laser cavity [14]. Once the inversion grating has been defined, it is straightforward to divide the gain among the longitudinal modes as in (3) and subsequently formulate the rate equations.

To give an overview of the different dynamics that can be extracted from the model, we performed a stability analysis for a two-active modes scenario. It was shown that many different behaviors are possible, e.g., single-mode CW operation, multimode cooperation in two longitudinal modes, and bistable behavior between different CW states (modes). The diversity of the dynamics was illustrated in Fig. 1, where we indicated the different dynamical regimes in the $(\Delta J, \delta f_{k,l})$-plane.

Then we calibrated the model using measurements from a real laser constructed in the European FALCON-TMR network. After demonstrating the calibration/extraction process of the model parameters, we reproduced a PI curve of the laser, where the intra-mode dynamics were chosen by adjusting the inversion-modal weights, i.e., the $f_{k,l}$ coefficients.

The model presented can be applied to many different types of semiconductor lasers. As we have shown, the design of the laser (cavity structure and gain profile) can be accounted for through the $f_{k,l}$'s, which also induce the gain dynamics. It was realized from (16) that the ratio of the modal weights ($f_{k,l}$'s) will be decisive for the type of mode competition. To reproduce a multimode laser, the modal weights must be such that all the longitudinal modes have a well-defined inversion moment, i.e., $f_{k,k}$ must be larger than $f_{j,k}$, where $j \neq k$ for all active modes. In this scenario, each longitudinal mode will behave as a Lang–Kobayashi type of mode with a weak coupling to the side modes through the inversion. To simulate the other extreme, a strong monomode laser like for example a DFB-type laser, one needs to define a dominant mode and set the modal weights such that the dominant mode will deplete the inversion of all other modes. This can be achieved by setting $f_{k,k} > f_{j,k}$ for the dominant mode and $f_{k,k} < f_{j,k}$ for the side modes. Also, the self-modal weight ($f_{k,k}$) of the dominant mode must be larger than the self-modal weight of the side modes. In this manner, there exists one "global" inversion (that of the dominant mode) and all modes feed from it with the dominant mode getting the most. In future work, we will apply this model to the twin-stripe lasers [7], [16] in order to reproduce the high-frequency dynamics that were predicted [18], [19].

References

[1] R. Lang and K. Kobayashi, "External optical feedback effects on semiconductor injection laser properties," *IEEE J. Quantum Electron*, vol. QE-16, pp. 347–355, 1980.

[2] J. Mørk, B. Tromborg, and J. Mark, "Chaos in semiconductor lasers with optical feedback: Theory and experiment," *IEEE J. Quantum Electron.*, vol. 28, pp. 93–108, 1992.

[3] G. H. M. van Tartwijk, A. M. Levine, and D. Lenstra, "Sisyphus effect in semiconductor lasers with optical feedback," *IEEE J. Select. Topics Quantum Electron.*, pp. 466–472, 1997.

[4] I. Fischer, G. H. M. van Tartwijk, A. M. Levine, W. E. Elsässer, E. Göbel, and D. Lenstra, "Fast pulsing and chaotic itinerancy with a drift in the coherence collapse of semiconductor lasers," *Phys. Rev. Lett.*, vol. 76, pp. 220–223, 1996.

[5] S. Wieczorek, B. Krauskopf, and D. Lenstra, "A unifying view of bifurcations in a semiconductor laser subject to optical injectiion," *Opt.Comm.*, vol. 172, pp. 279–295, 1999.

[6] K. Petermann, *Laser Diode Modulation and Noise*. Dordrecht, The Netherlands: Klüwer, 1988.

[7] M. Yousefi, A. Barsella, D. Lenstra, G. Morthier, and R. Baets, "On the role of longitudinal mode dynamics in laterally coupled lasers," in *Proc. SPIE*, vol. 4646, 2002, pp. 388–396.

[8] W. W. Chao, S. W. Koch, and M. Sargent III, *Semiconductor-Laser Physics*. Berlin, Germany: Springer-Verlag, 1994.

[9] B. Krauskopf and D. Lenstra, "Fundamental issues of nonlinear laser dynamics," in *AIP Conf. Proc.*, vol. 548, Texel, The Netherlands, 2000.

[10] C. Simmendinger, D. Prefißer, and O. Hess, "Stabilization of chaotic spatiotemporal filamentation in large broad area lasers by spatial optical feedback," *Opt. Exp.*, vol. 5, no. 3, pp. 48–54, 1999.

[11] H. F. Hofmann and O. Hess, "Quantum Maxwell-Bloch equations for spatially inhomogeneous semiconductor lasers," *Phys Rev. A*, vol. 59, pp. 2342–2358, 1999.

[12] S. H. Strogatz, *Nonlinear Dynamics and Chaos*. New York: Perseus, 2000.
[13] C. H. Henry, "Theory of linewidth of semiconductor lasers," *IEEE J. Quantum Electron*, vol. QE-18, pp. 259–263, 1982.
[14] T. W. Carr, D. Pieroux, and P. Mandel, "Theory of a multimode semiconductor laser with optical feedback," *Phys. Rev. A*, vol. 63, 2001.
[15] W. H. Press, S. A. Teukolsky, W. T. Vetterling, and B. P. Flannery, *Numerical Recipes in C*. New York: Cambridge Univ. Press, 1994.
[16] S. McMurtry, J.-P. Vilcot, F. Mollot, and D. Decoster, "Farication and characterization of laterally coupled lasers," in *Proc. SPIE*, vol. 4646, 2002, pp. 367–374.
[17] G. P. Agrawal and N. K. Dutta, *Long Wavelength Semiconductor Lasers*. New York: Van Nostrand Reinhold, 1986.
[18] H. Lamela, B. Roycroft, P. Acedo, R. Santos, and G. Carpintero, *Opt. Lett.*, vol. 27, pp. 303–305, 2002.
[19] H. Lamela, M. Leonés, G. Carpintero, C. Simmendinger, and O. Hess, *IEEE J. Select. Topics Quantum Electron.*, vol. 7, pp. 192–199, 2001.

Mirvais Yousefi was born in Kabul, Afghanistan, in 1975. He received the M.Sc. degree from the University of Lund, Lund, Sweden, in 1998 and the Ph.D. degree from the Vrije Universiteit of Amsterdam, Amsterdam, The Netherlands, in 2003. The focus of his research was on the analysis of the dynamics of coupled semiconductor lasers in several configurations, such as filtered feedback and laterally coupled semiconductor lasers.

Since January 2003, he has been with the Vrije Universiteit of Amsterdam, analyzing the influence of noise on the dynamics of semiconductor lasers.

Dr. Yousefi received the IEEE-LEOS Graduate Student Fellowship in 2001.

Alberto Barsella graduated in physics from the University of Pisa, Pisa, Italy, in 1994, and received the Ph.D. degree in physics from the University of Lille, Lille, France, in 2000. His research focused on nonlinear optics and laser dynamics.

Since 2000, he has been with the University of Gent, Gent, Belgium, as a post-doctorate Researcher, working on the dynamics of coupled semiconductor lasers and tunable lasers.

Daan Lenstra (M'97) was born in Amsterdam, The Netherlands, in 1947. He received the M.Sc. degree in theoretical physics from the University of Groningen, Groningen, The Netherlands, and the Ph.D. degree from Delft University of Technology, Delft, The Netherlands. His thesis work was on polarization effects in gas lasers.

Since 1979, he has researched topics in quantum electronics, laser physics, and condensed matter physics. In 1991, he joined the Vrije Universiteit, Amsterdam, The Netherlands, holding a Chair in theoretical quantum electronics. Since September 2000, he has also been a part-time Professor at the Department of Electrical Engineering, Eindhoven University of Technology, Eindhoven, The Netherlands. His areas of research include nonlinear and ultra-fast dynamics of semiconductor optical amplifiers and diode lasers, quantum optics in small semiconductor structures, and near-field optics. He has coauthored more than 170 publications in international scientific journals and co-edited six books and special journal issues.

Geert Morthier (M'93–SM'01) received the electrical engineering degree and the Ph.D. degree from Gent University, Gent, Belgium, in 1987 and 1991, respectively.

During 1998–1999, he was the Project Manager of the ACTS project ACTUAL, dealing with the control of widely tunable laser diodes. Since 1991, he has been a member of the permanent staff of IMEC, Gent, Belgium, and since 2001, he has been the Project Manager of the IST project NEWTON, which focuses on new widely tunable lasers. He was appointed part-time Professor at the Gent University in 2001. His main interests are in the modeling and characterization of optoelectronic components. He has authored or co-authored around 100 papers in the field. He is also one of the two authors of the *Handbook of Distributed Feedback Laser* (Norwood, MA: Artech House, 1997) and co-editor of the book *How to Model and Measure Photonic Components: Experience from a European Project* (Berlin, Germany: Springer-Verlag, 1998).

Roel Baets (M'88) received the electrical engineering degree from Gent University, Gent, Belgium, in 1980, the M.Sc. degree in electrical engineering from Stanford University, Stanford, CA, in 1981, and the Ph.D. degree from Gent University, Gent, Belgium, in 1984.

Since 1981, he has been with the Department of Information Technology (INTEC), Gent University, where since 1989, he has been a Professor in the Engineering Faculty. From 1990 to 1994, he was a part-time Professor at the Technical University of Delft, Delft, The Netherlands. He has worked in the field of III-V devices for optoelectronic systems. Through about 300 publications and conference papers, he has made contributions to the design and fabrication of semiconductor laser diodes, passive guided-wave devices, PICs, and microoptic components. He leads the Optoelectronic Components and Systems group at Gent University-INTEC (an associated lab of IMEC), working on photonic devices for optical communication and optical interconnect.

He was Chairman of the lEEE Lasers and Electro-Optics Society (LEOS)-Benelux chapter from 1999 to 2001. He is a member of the Optical Society of America, IEEE-LEOS, SPIE, and the Flemish Engineers Association. He has been a member of the program committees of OFC, ECOC, the IEEE Semiconductor Laser Conference, ESSDERC, CLEO-Europe, and he European Conference on Integrated Optics.

Stefan McMurtry, photograph and biography not available at the time of publication.

Jean-Pierre Vilcot, photograph and biography not available at the time of publication.